Supplement of Atmos. Chem. Phys., 22, 4895–4907, 2022
https://doi.org/10.5194/acp-22-4895-2022-supplement

Atmospheric Chemistry and Physics
Open Access
EGU

Supplement of

The impact of molecular self-organisation on the atmospheric fate of a cooking aerosol proxy

Adam Milsom et al.

Correspondence to: Christian Pfrang (c.pfrang@bham.ac.uk)

S1. Model reaction scheme

(R1) O_3 + oleic acid → c(NN + CI) + (1-c)(C_9 + CI)

(R2) CI + C9 → dimer

(R3) CI + dimer → trimer

A simplified form of the reaction scheme used by Hosny *et al*. has been used (Hosny et al., 2016). The initial reaction of oleic acid with ozone (O_3) forms nonanal (NN) or a 9-carbon (C_9) product (nonanoic acid, 9-oxononanoic acid or azelaic acid) plus a Criegee intermediate (CI). The relative amount of NN and C_9 products is determined by the branching ratio (c). We have also included the loss of NN from the surface due to its high volatility. The CI then goes onto react with a C_9 product to form the dimer. This dimer then reacts with another CI to form the trimer, which represents all higher order products in this model scheme.

Since this is a simplified reaction scheme and we assume that diffusion parameters dominate the reaction kinetics, we have held all reaction rates to those optimised by Hosny et al. (Hosny et al., 2016) (see next section).

S2. Model parameters

Parameter	*Description*	*Value*	*Units*
$k_{BR,1}$	Bulk reaction rate coefficient for R1	1.13×10^{-18}	$cm^3\ s^{-1}$
$k_{BR,2}$	Bulk reaction rate coefficient for R2	1.86×10^{-17}	$cm^3\ s^{-1}$
$k_{BR,3}$	Bulk reaction rate coefficient for R3	1.99×10^{-16}	$cm^3\ s^{-1}$
c	Stoichiometric coefficient (branching ratio)	0.454	
$H_{cp,O3}$	Henry's law coefficient of O3 in organics	6.66×10^{-4}	mol cm^{-1} atm
$T_{d,O3}$	Surface desorption lifetime of O3	1.67×10^{-7}	s
$\alpha_{s,0}$	Surface accommodation coefficient of O3	0.13	
D_{dimer}	Bulk diffusion coefficient of the dimer	$[1.03 \times 10^{-12}]$	$cm^2\ s^{-1}$
f_{diff}	Power law scaling factor for oligomer viscosity	3.96	
$D_{X,lam}$	Bulk diffusion coefficient of O_3 in the lamellar phase	$[3.35 \times 10^{-12}]$	$cm^2\ s^{-1}$
$D_{Y,lam}$	Bulk diffusion coefficient of oleic acid in the lamellar phase	$[2.81 \times 10^{-12}]$	$cm^2\ s^{-1}$
$D_{X,di}$	Bulk diffusion coefficient of O_3 in the dimer	$[4.66 \times 10^{-9}]$	$cm^2\ s^{-1}$
$D_{Y,di}$	Bulk diffusion coefficient of oleic acid in the dimer	$[8.85 \times 10^{-11}]$	$cm^2\ s^{-1}$
$D_{X,tri}$	Bulk diffusion coefficient of O_3 in the trimer	$[1.49 \times 10^{-12}]$	$cm^2\ s^{-1}$
$D_{Y,tri}$	Bulk diffusion coefficient of oleic acid in the trimer	$[8.16 \times 10^{-11}]$	$cm^2\ s^{-1}$
f_{slr}	Scaling factor for surface reaction rates	4.41×10^{6}	cm^{-1}
$k_{loss,NN}$	Rate of nonanal loss from particle surface	1.4	s^{-1}
ω_X	Mean thermal velocity of O_3	3.6×10^{4}	cm s^{-1}

Table S1. Parameters used in the model. Parameters in square brackets were optimised using the differential evolution global optimisation algorithm.

All unvaried parameters are constrained to the values reported by Hosny *et al.* (Hosny et al., 2016) except for the rate of nonanal loss from the particle surface ($k_{loss,NN}$), which was found not to affect the model output under these conditions and set to a value of 1.4 s^{-1}.

	Film thickness / μm			
	0.59	***0.91***	***0.98***	***1.66***
$D_{x,lam}$	4.58×10^{-12}	1.13×10^{-12}	8.78×10^{-10}	5.64×10^{-12}
$D_{x,tri}$	5.64×10^{-10}	3.42×10^{-9}	9.76×10^{-9}	9.12×10^{-9}
$D_{Y,lam}$	8.45×10^{-13}	1.08×10^{-12}	7.32×10^{-13}	5.54×10^{-12}
$D_{Y,tri}$	1.24×10^{-11}	1.33×10^{-11}	9.88×10^{-11}	4.89×10^{-11}
D_{di}	4.20×10^{-10}	9.49×10^{-10}	6.33×10^{-10}	6.28×10^{-10}
$D_{x,di}$	7.34×10^{-9}	2.14×10^{-9}	3.86×10^{-9}	7.75×10^{-9}
$D_{Y,di}$	7.92×10^{-11}	5.03×10^{-11}	9.93×10^{-11}	8.85×10^{-11}

Table S2. Diffusion parameters optimised for individual fits to each separate experimental decay data presented in Fig. 1 of the main text. All values are in units of $cm^2\ s^{-1}$.

S3. Film composition evolution for liquid oleic acid model run

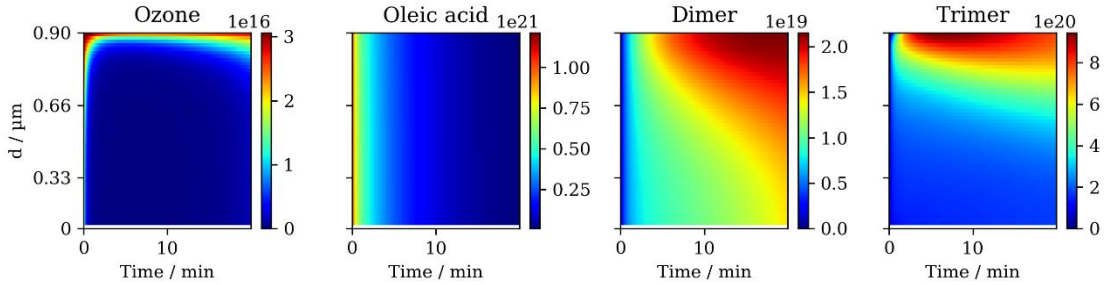

Figure S1. Evolution of component concentration for model runs using liquid oleic acid diffusivity parameters described in the main text. d: distance from the film core. $[O_3]$ = 77. ppm. Concentrations are in cm^{-3}.

S4. 2-D SAXS pattern of a coated capillary

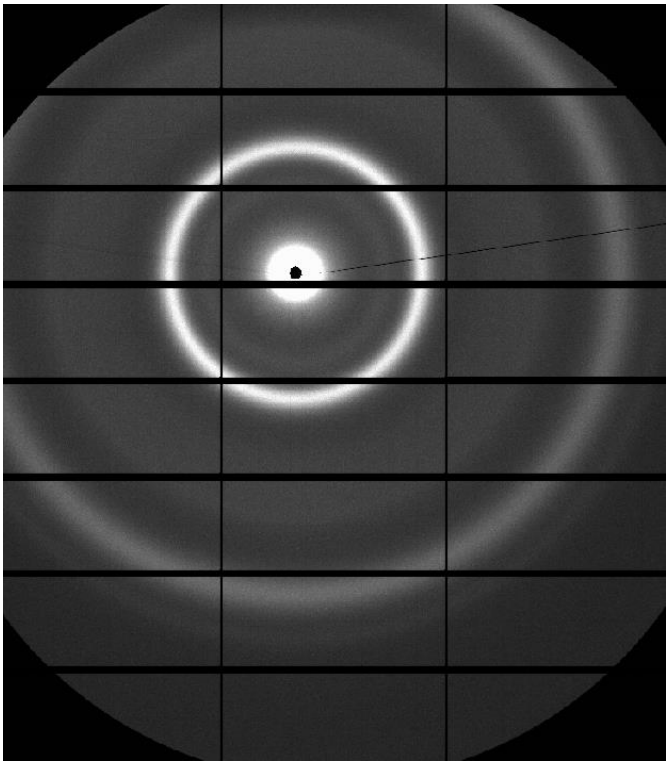

Figure S2. 2-D SAXS pattern of a capillary coated with the oleic acid-sodium oleate (1:1 wt) proxy, showing diffuse scattering rings. The outer ring arises from the Kapton detector window.

The 2-D scattering pattern from the experiment used in this modelling study exhibits diffuse scattering rings with an even intensity (see the most intense scattering ring in Fig. S2) (Milsom et al., 2021). There are no regions of increased scattered intensity around each scattering ring, therefore the lamellae in are randomly oriented. Lamellar phase orientation would result in either a “spotty” scattering ring or a scattering ring where only certain opposing arcs are visible.

S5. Model iterations and sensitivity to fixed parameters

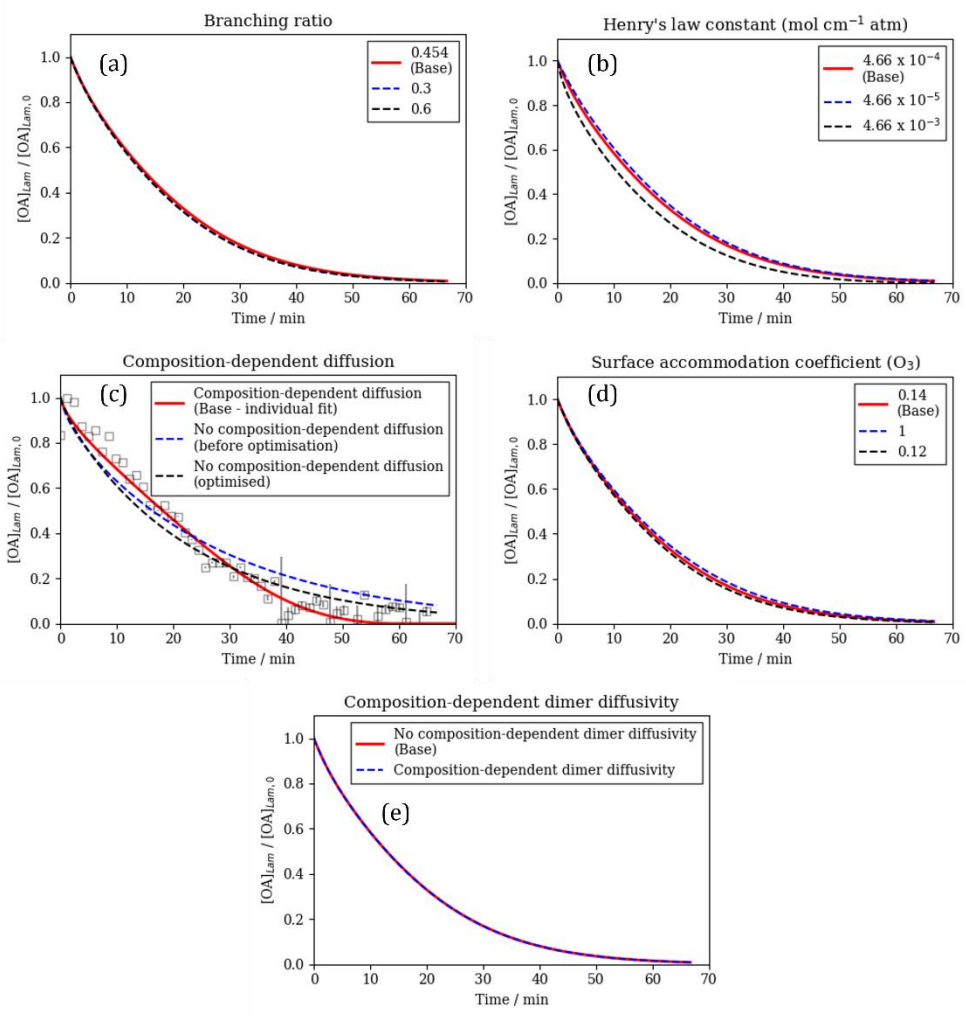

Figure S3. (a) The effect of the branching ratio for reaction R1 on the model output. (b) The effect of Henry's law constant for ozone ($H_{cp,O3}$) on the model output. (c) Comparison between composition-dependent and non-composition dependent diffusion. (d) The effect of the surface accommodation coefficient for ozone ($\alpha_{s,0}$) on the model output. All plots are model outputs for a 0.98 µm film. (e) Comparing model outputs with and without composition-dependent dimer diffusivity. "Base" stands for the model output from optimisation to all datasets simultaneously (see Fig. 2, main text).

References

Hosny, N. A., Fitzgerald, C., Vyšniauskas, A., Athanasiadis, A., Berkemeier, T., Uygur, N., Pöschl, U., Shiraiwa, M., Kalberer, M., Pope, F. D. and Kuimova, M. K.: Direct imaging of changes in aerosol particle viscosity upon hydration and chemical aging, Chem. Sci., 7(2), 1357–1367, doi:10.1039/c5sc02959g, 2016.

Milsom, A., Squires, A. M., Woden, B., Terrill, N. J., Ward, A. D. and Pfrang, C.: The persistence of a proxy for cooking emissions in megacities: a kinetic study of the ozonolysis of self-assembled films by simultaneous small and wide angle X-ray scattering (SAXS/WAXS) and Raman microscopy, Faraday Discuss., 226, 364–381, doi:10.1039/D0FD00088D, 2021.